Tellus
SERIES A
DYNAMIC
METEOROLOGY
AND OCEANOGRAPHY
PUBLISHED BY THE INTERNATIONAL METEOROLOGICAL INSTITUTE IN STOCKHOLM

Tellus (2011), 63A, 876–883
Printed in Singapore. All rights reserved

TELLUS

Response of precipitation extremes to idealized global warming in an aqua-planet climate model: towards a robust projection across different horizontal resolutions

By FUYU LI[1]*, WILLIAM D. COLLINS[1], MICHAEL F. WEHNER[1], DAVID L. WILLIAMSON[2] and JERRY G. OLSON[2], [1]*Lawrence Berkeley National Laboratory, 1 Cyclotron Road, MS 50A4037, Berkeley, CA 94720, USA;* [2]*National Center for Atmospheric Research, Boulder, CO, USA*

(Manuscript received 30 November 2010; in final form 18 July 2011)

ABSTRACT

Current climate models produce quite heterogeneous projections for the responses of precipitation extremes to future climate change. To help understand the range of projections from multimodel ensembles, a series of idealized 'aquaplanet' Atmospheric General Circulation Model (AGCM) runs have been performed with the Community Atmosphere Model CAM3. These runs have been analysed to identify the effects of horizontal resolution on precipitation extreme projections under two simple global warming scenarios. We adopt the aquaplanet framework for our simulations to remove any sensitivity to the spatial resolution of external inputs and to focus on the roles of model physics and dynamics. Results show that a uniform increase of sea surface temperature (SST) and an increase of low-to-high latitude SST gradient both lead to increase of precipitation and precipitation extremes for most latitudes. The perturbed SSTs generally have stronger impacts on precipitation extremes than on mean precipitation. Horizontal model resolution strongly affects the global warming signals in the extreme precipitation in tropical and subtropical regions but not in high latitude regions. This study illustrates that the effects of horizontal resolution have to be taken into account to develop more robust projections of precipitation extremes.

1. Introduction

Major changes in hydrological cycle are expected with the strong increase of atmospheric water vapour content under global warming. Particularly, the warming of the climate will likely lead to increases in the intensities and frequencies of extreme precipitation events, which result from anomalous horizontal moisture flux convergence (Trenberth et al., 2003; Held and Soden, 2006; O'Gorman and Schneider, 2009). Significant trends in precipitation extremes have been detected in conjunction with the observed warming of the climate in recent decades (Schneider and O'Gorman, 2007). Global rainfall data sets, based on blended space- and ground-based measurements, show a significant positive trend in the occurrence of heavy rain events during the period 1979–2003 (Lau and Wu, 2007). Kharin et al. (2007) found a 6% K^{-1} increase in the 20-year return period precipitation associated with increased global-mean surface temperature in coupled climate simulations of global warming. Goswami et al. (2006) also reported significant rising trends in the frequency and magnitude of extreme rain events over central India during the monsoon seasons from 1951 to 2000. The enhancement of extreme precipitation with global warming could be caused by enhancement of atmospheric moisture content (Trenberth, 1999), but it may not scale with the increase of water vapour content or mean precipitation because of the redistribution of heat and water vapour due to the compensation of large- and local-scale air motions (Allen and Ingram 2002). Several studies (e.g. Cubasch et al., 2001; Pall et al., 2007) project larger and faster increases in the extreme precipitation relative to mean precipitation, and this could cause more frequent and severe floods in future warmer climates. Detectible increases in extreme precipitation have also been recently attributed to human activities (Min et al. 2010).

However, the ability of the current generation of climate models to simulate and project these extreme precipitation events is still an open question at present (Randall et al., 2007). First of all, the moist convective parameterizations are not necessarily designed to capture high-order statistics of rainfall. The differences between the simulations of precipitation extremes using two different convection schemes are larger than those

*Corresponding author:
e-mail: fli@lbl.gov
DOI: 10.1111/j.1600-0870.2011.00543.x

from 2° surface warming using either scheme (Wilcox and Donner, 2007). Secondly, the mechanisms for the precipitation extremes are still poorly understood (O'Gorman and Schneider, 2009). The climate models may fail to accommodate the essential mechanisms that lead to extreme weather events (Sun et al., 2006). Also, simulations of precipitation extremes appear to depend on free parameters in the model configurations, in particular the horizontal resolution. Although finer lateral grids have improved the statistics of precipitation intensity (Boyle and Klein, 2010; Wehner et al., 2010), simulations of precipitation extremes need not converge with increasing model resolution (Williamson, 2008b; Li et al., 2011).

All of the above issues could contribute to systematic errors in projections of precipitation extremes. It is clear that more effort is necessary to document the changing characteristics of rainfall under global warming scenarios. Although the convergence of extreme projection itself would not be possible until the physics and dynamics that govern the precipitation extremes converge across climate models, this study will specifically investigate the 'resolution convergence' issue, that is the effect of horizontal resolution on projections of future weather extreme changes in climate models. We will concentrate on an idealized model configuration subjected to several simplified warming scenarios. The descriptions of the model and experimental design are presented in Section 2. Section 3 shows the results of the simulations for control simulation (Section 3.1); the responses of precipitation extremes to global warming scenarios under standard climate model setups at four horizontal resolutions (Sections 3.2 and 3.3); the impact of horizontal resolutions on the projections when considering just larger spatial scales (Section 3.4) and some possible explanations for the responses (Section 3.5). We then present our conclusions in Section 4.

2. Model description

A series of AGCM runs using the NCAR Community Atmospheric Model Version 3.0 (CAM3; Collins et al., 2004) have been performed with highly simplified and idealized 'aquaplanet-steady-state' boundary conditions. Details of the model have been described in Li et al. (2011) along with some aspects of the control simulation used in the following analysis. The atmospheric stand-alone simulations use the standard CAM Eulerian spectral transform dynamical core and the experiments are performed at four horizontal resolutions corresponding to spectral truncations of T42, T85, T170 and T340 (∼2.8°, 1.4°, 0.7° and 0.35° transform grids, respectively). The standard operating mode for the Eulerian dynamical core requires decreasing time steps with increasing horizontal resolution to maintain numerical stability in accordance with the CFL criterion (Courant et al., 1928, 1967). The time steps are accordingly set to 40, 20, 10 and 5 min for the T42, T85, T170 and T340 spectral truncations in the simulations analysed later. The simulation periods are 8, 4, 2 and 2 yr for all the control and warming runs at T42, T85, T170 and T340 respectively, with 1-year 'spin up' period. As stated in our previous study (Li et al., 2011), the model transitions from its initial conditions to its aqua-planet climate in less than 2 months (Williamson, 2008b). The inverse relationship between spatial resolution and simulation period is to take advantage of the zonal symmetry in aqua-planet world by the doubling of the number of grid points in the zonal direction with each refinement in resolution. The sampling sizes are sufficient to maintain the simulation errors below desirable levels for most of the extreme events such as the 95th percentile extreme precipitation used in this study. See Li et al. (2011) for further discussion of this sampling.

The model configuration adopted for our runs has been developed under the framework of Aqua-Planet Experiment Project (APE; Neale and Hoskins, 2000). In the APE experimental protocol, the entire planetary surface is treated as an ocean with specified zonally symmetric sea-surface temperatures (SST). This protocol eliminates the resolution-dependent signals from external boundary conditions and helps isolate the internal physical and dynamical mechanisms driving the changes of precipitation extremes in response to global warming.

The prescribed zonally symmetric SST field proposed by Neale and Hoskins (2000) is used for the control conditions (black line in Fig. 1):

$$\mathrm{SST}(\varphi) = \begin{cases} 27\left(1 - \sin^2\left(\frac{90}{60}\varphi\right)\right) & \text{if} \quad |\varphi| < 60^\circ, \\ 0 & \text{if} \quad |\varphi| > 60^\circ, \end{cases} \tag{1}$$

where SST is in units of °C and φ is the latitude ranging from −90° to 90°.

Two simple scenarios are defined, one to mimic the effects of increasing low-to-high latitude SST gradient (denoted by 'sstgra') and the other to mimic increased SST magnitude ('sstmag') in response to global warming. In experiment 'sstgra', we increase the maximum SST at equator by 3 °C from 27 to 30 °C while leaving the high-latitude SSTs unchanged from the control conditions (eq. 2) as shown by the red line in Fig. 1. In experiment 'sstmag', we apply a uniform 3 °C increase of SST

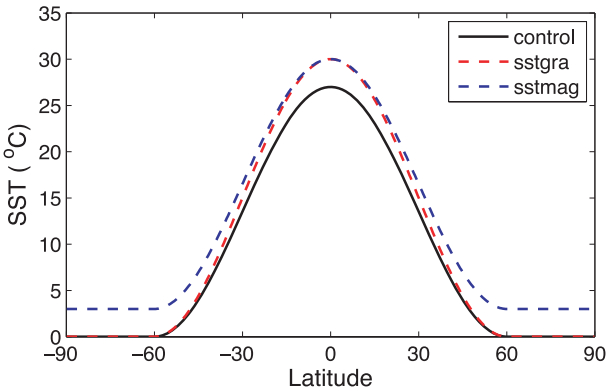

Fig. 1. Prescribed SST distributions for the control and two global warming experiments: control (black), sstgra (red) and ssmag (blue).

at all latitudes (eq. 3) as shown by the blue line in Fig. 1.

$$\mathrm{SST}(\varphi) = \begin{cases} 30\left(1 - \sin^2\left(\frac{90}{60}\varphi\right)\right) & \text{if} \quad |\varphi| < 60^\circ, \\ 0 & \text{if} \quad |\varphi| > 60^\circ, \end{cases} \tag{2}$$

$$\mathrm{SST}(\varphi) = \begin{cases} 3 + 27\left(1 - \sin^2\left(\frac{90}{60}\varphi\right)\right) & \text{if} \quad |\varphi| < 60^\circ, \\ 3 & \text{if} \quad |\varphi| > 60^\circ. \end{cases} \tag{3}$$

Note that we are making the simplest possible modifications of the prescribed SST based on the SST profiles defined by Neale and Hoskins (2000) in the APE protocol (cf. http://www.reading.ac.uk/m̃ike/APE/ape_home.html) rather than prescribing more realistic meridional perturbations to the background climatology. Our modifications do not necessarily mimic more detailed projections of the patterns of climate change in which the polar regions warm more than the tropics and hence the latitudinal SST gradients are smaller than those in 'sstgra' and 'sstmag'. However, the effect of real-world stronger polar-warming scenarios could be inferred from the difference between 'sstgra' (larger latitudinal SST gradient) and 'sstmag' (smaller latitudinal gradient).

The results from the above experiments are analysed to investigate the response of precipitation extremes to the idealized global warming. The extreme precipitation index used in this study is the annual total 95% percentile wet-day precipitation (here after: R95pTOT), which is based on Frich indices (Frich et al., 2002; Alexander et al. 2006) and has been described in detail in Li et al. (2011). R95pTOT is calculated by summing over an annual cycle all the daily precipitation larger than the 95% percentile of the climatological daily precipitation in wet-days, defined as daily precipitation larger than 1 mm d^{-1}.

Because the insolation is held fixed in an equinoctial and hemispherically symmetric geometry, and because the radiatively active species are set to zonally and temporally invariant concentrations and are hemispherically symmetric, the statistics of the simulation climate are zonally and hemispherically symmetric. In the analysis later, the two hemispheres are treated as two independent samples and averaged together to increase the signals of climate change relative to internal unforced variability and to simultaneously reduce the computations required for robust statistics. All the results are shown in the equivalent Northern Hemisphere equator to pole domain. To distinguish the strong signals near the equator, different latitude scales are used (smaller meridional intervals for the low latitudes and larger intervals for mid-high latitudes) in all the figures in this study.

3. Results

3.1. Control experiment

The control simulations are the same as the runs performed in Li et al. (2011). Figure 2 shows the mean and extreme precipitation from four resolutions with transform grids spanning 0.35–2.8°

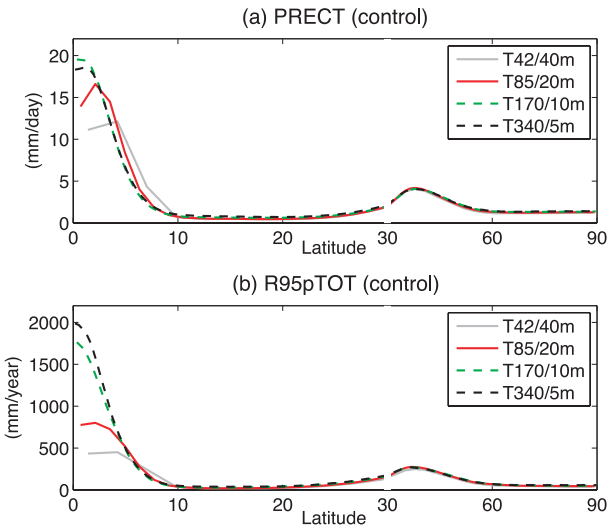

Fig. 2. Zonal-mean daily (a) mean precipitation and (b) extreme precipitation for control simulations based on standard CAM configurations at four resolutions. Note the changes of latitude scales at 30° and the different units for the two fields.

on the equator. We have used the standard mode of running the spectral Eulerian version of CAM by decreasing the time step from 40 to 5 min as the grid changes from T42 to T340. As Li et al. (2011) have shown, both the horizontal resolution and the model time step affect the convergence of the mean and extreme precipitation after averaged onto the same coarser grid. We only describe some features relevant to this study here.

Both mean and extreme precipitation show local maxima near the equator and at mid-latitude regions analogous to the Intertropical Convergence Zone and storm tracks in the Earth's climate system. The differences in these fields across the four different resolutions are evident in tropics but much smaller for higher latitudes. In the tropics, the daily mean precipitation generally increases with increasing horizontal resolution from T42 to T170 with a slight decrease at T340 (Fig. 2a). There are daily mean precipitation minima over two grid points at the equator for T42 and T85, creating the 'double maxima' features, which are less obvious for the extreme precipitation. The equatorial precipitation minimum is still a poorly understood issue and some of the causes have been discussed in Williamson and Olson (2003) and Williamson (2008a). This precipitation minimum is not observed under most of the global warming simulations presented here and it contributes to some of the strong warming signals seen with T42 and T85 simulations, which will be discussed later.

Although the extreme precipitation is a localized phenomenon and not always very organized by large-scale dynamics, the increasing horizontal resolution, by default, would resolve more extreme precipitation and result in the increase seen in Fig. 2b. However, the addition of smaller grids contributes to only part of the resolution dependency signals, and as discussed in more

details in Li et al. (2011), the extreme precipitation does not converge even after averaging onto the same coarser grids. We will specifically target this 'resolution-convergence' issue of projections in Section 3.4, which also eliminates the effects from the changing time steps in the standard mode of GCM simulations. In Sections 3.2 and 3.3, we will focus on the projection signals from the standard mode of GCM runs at their original girds and time steps.

3.2. *Experiment with greater SST gradients*

The 'sstgra' experiment mimics the effect of increasing the low-to-high latitude SST gradient (red line in Fig. 1) by increasing the maximum prescribed SST by 3 °C at the equator while holding the polar values fixed. Figure 3a and b show the absolute values of mean and extreme precipitation at four resolutions under 'sstgra' conditions. Figure 3c shows the changes of extreme precipitation relative to their values in the control experiment at corresponding resolutions (Fig. 2). Under 'sstgra' conditions, the daily mean precipitation increases with increasing resolution in tropics as also seen in the control experiment (Fig. 2). The maximum precipitation at the equator is getting narrower but without the minima associated with the double structure in the control. The extreme precipitation is more sensitive to horizontal resolution compared to the mean precipitation. The extreme precipitation at the lower T42 and T85 resolutions is significantly smaller than the extreme precipitation at the higher T170 and T340 resolutions, similar to that in the control simulations but with much higher precipitation rates. For instance, the extreme precipitation at T42 is less than one-fourth of that for T170 (Fig. 3b). The perturbed SST generally has stronger impacts on precipitation extremes compared with mean precipitation.

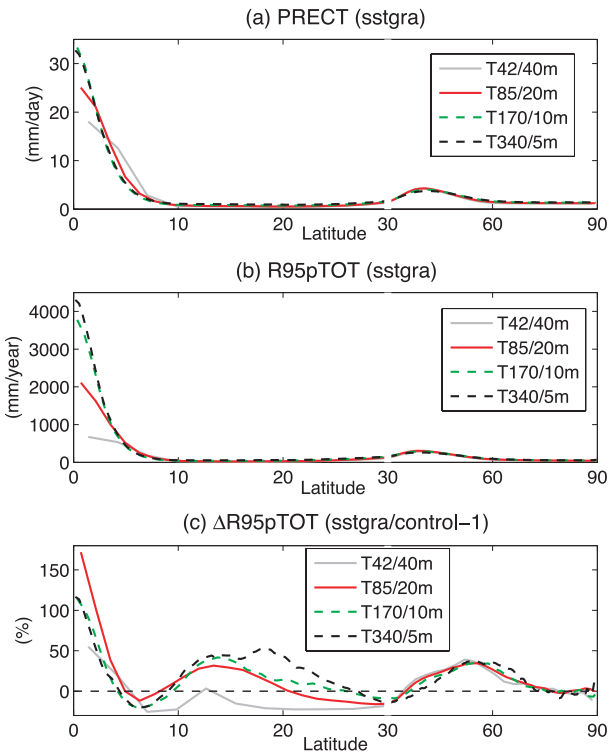

Fig. 3. Zonal-mean daily (a) mean precipitation, (b) extreme precipitation and (c) the change of extreme precipitation relative to control simulation, for the "sstgra" experiment performed at four resolutions. Note the changes of latitude scales at 30° and the different units for the two fields.

Compared to control conditions, the 'sstgra' warming scenario results in the increase of extreme precipitation in three major tropical and extratropical regions. The extreme precipitation increases by up to 150% at the equator and by nearly 50% in latitudes between approximately 10–20° and 50–60° in both hemispheres for almost all the resolutions except T42. The extreme precipitation decreases at approximately 6–7° due to the enhancement of convection at equator and a strengthening and narrowing of the upward branch of the Hadley cell. At approximately 30° it decreases due to the less moisture available in this region to form precipitation, and this is consistent with the 'dry-gets-drier' pattern reported in many previous studies (e.g. Held and Soden, 2006). The mean precipitation decreases by 30–40% at the subtropical downdraft zone (not shown).

The projected relative changes in extreme precipitation under the 'sstgra' warming scenario are affected by horizontal resolution in the low mid-latitudes but are relatively insensitive to resolution in high latitude regions (Fig. 3c). Although the T170 and T340 simulations show consistent signals at the equator, the increase of the extreme precipitation is much lower in T42. The T85 experiment yields the highest percentage increase at the equator primarily due to the different structures in the precipitation at the equator (Fig. 2b). The control simulation has an equatorial minimum associated with the double ICTZ whereas 'sstgra' has a single maximum on the equator. For the subtropics, the T42 run shows a decrease of extreme precipitation whereas the other three resolutions show an increase. Slight differences are also seen between different resolutions for other subtropical regions. Note that between ∼10° and 30°, the absolute values of mean and extreme precipitation are very small, and hence the large relative differences among the simulations at various resolutions in this region do not appreciably affect the total amounts of precipitation.

3.3. *Experiment with uniformly greater SSTs*

Figure 4 shows the mean, extreme precipitation and changes of extreme precipitation, relative to control experiment at corresponding resolutions, for the increased SST magnitude experiment 'sstmag'. Under the 3 °C uniform warming globally, the mean and extreme precipitation at the equator are much less than those under 'sstgra' conditions, particularly for the higher resolutions T170 and T340 (Figs 4a and b). In contrast to the control simulations, there are no equatorial minima although

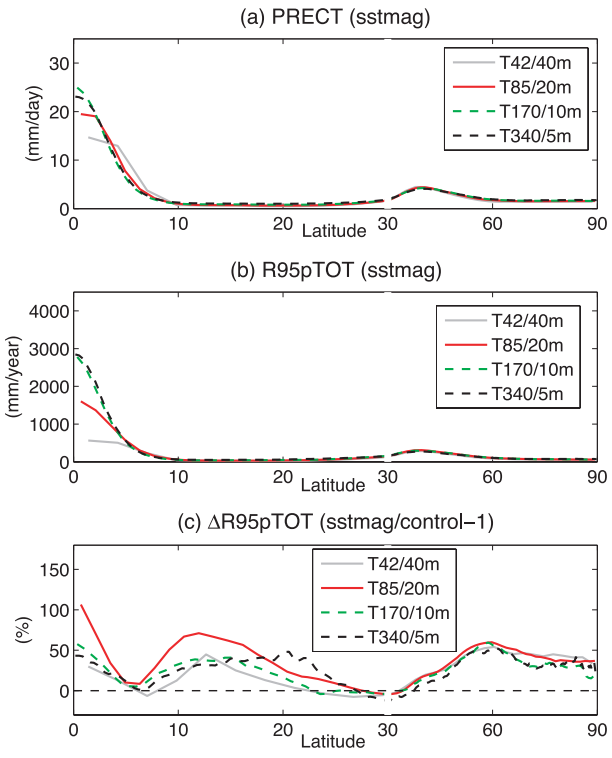

Fig. 4. The same as Fig. 3 but for 'sstmag' experiment.

T42 and T85 are relatively wide and flat there, The relative increase of extreme precipitation is ∼50% for T42, T170 and T340 and ∼100% for T85 (Fig. 4c). Again, the T85 relative increase is affected by the different structures in the fields in the two experiments.

Figure 4c shows the similar trends for the change of extreme precipitation, compared to experiment 'sstgra' (Fig. 3c). Many regions experience an approximately 50% increase in the extreme precipitation, including the equatorial zone, the area between 10° and 25°, and the polar regions in both hemispheres. The changes are comparable to the increases observed under 'sstgra' conditions for mid-latitude regions but are much higher in polar regions, where SST is kept at 0 °C under 'sstgra' as opposed to 3 °C here in 'sstmag'. Although the regions near ∼30° become drier and are subject to lower mean precipitation, the extreme precipitation remains as the control simulation level. The T85 integration tends to project higher extreme precipitation under this warming scenario than the other resolutions. The impact of horizontal resolution on the projections of extreme precipitation is small for the other three horizontal resolutions.

In both warming scenarios, there is an increase of mean precipitation in the tropics and in mid- to high-latitudes and a decrease in subtropical regions for all the runs at different resolutions (not shown). This 'dry-gets-drier' pattern has also been reported in many previous studies with real-world simulations (e.g. Cubasch et al., 2001; Held and Soden, 2006). However, the extreme precipitation exhibits much more significant increases in the tropics and mid-high latitudes. This pattern is similar to the results from the ensemble of six couple ocean–atmosphere climate models established for the Intergovernmental Panel on Climate Change (IPCC) Fourth Assessment Report (AR4; Emori and Brown, 2005). The global-mean relative change in extreme precipitation of 13.0% is more than twice as large as that for mean precipitation.

3.4. *Impact of horizontal resolution*

One basic criterion for the robust and consistent projection precipitation extreme is that the projections should approach a fixed distribution once the model grid resolution approaches or exceeds the characteristic length for the phenomena of interest. We consider the projections to have converged at large scales if the larger scales are not affected by the addition of smaller scales in the model and the increasing horizontal resolution simply adds finer scales to the simulations. This issue has been specifically addressed in Li et al. (2011) for extreme precipitation and Williamson (2008b) for mean precipitation using the same model framework.

Figures 3 and 4 have shown how the projections of extreme precipitation in response to global warming change with increasing horizontal resolution and simultaneously decreasing time steps. This is not necessarily unexpected because the scales of the phenomena are decreasing. As discussed earlier, the time steps are required to change with the horizontal resolution to maintain dynamical stability (Courant et al., 1967). The time steps for T42, T85, T170 and T340 in the previous runs are 40, 20, 10 5 min., respectively. Because the time step also affects the precipitation and precipitation extremes (Williamson, 2008b; Li et al., 2011), we perform another set of simulations for T42, T85, T170 and T340, using the same setups as those for control, 'sstgra', 'sstmag' expect that the time steps are kept the same at 5 min. Figure 5 shows the changes of extreme precipitation under the two global warming scenarios 'sstgra' (Fig. 5a) and 'sstmag' (Fig. 5b) after averaging to the same low-resolution 5° grid to focus on the upscaled effects of resolution, using a mass-conservative and area-average method suggested by Chen and Knutson (2008). Note, the average is done on the original model data before the statistics are computed.

At high-latitude regions, the tendencies for increased extreme precipitation are similar to those shown in Figs 3c and 4c for the standard simulation configurations. There is no systematic resolution signal in the subtropics between 10° and 30°. The projections for T170 and T340 simulations in 'sstgra' match each other relatively well, but the projections clearly do not converge in 'sstmag', although the lack of convergence is probably due to the very low precipitation rate in this region. Near the equator, the changes of extreme precipitation are significantly lower than those in the standard mode. The projected fractional changes in precipitation extremes appear to converge at equator, with a

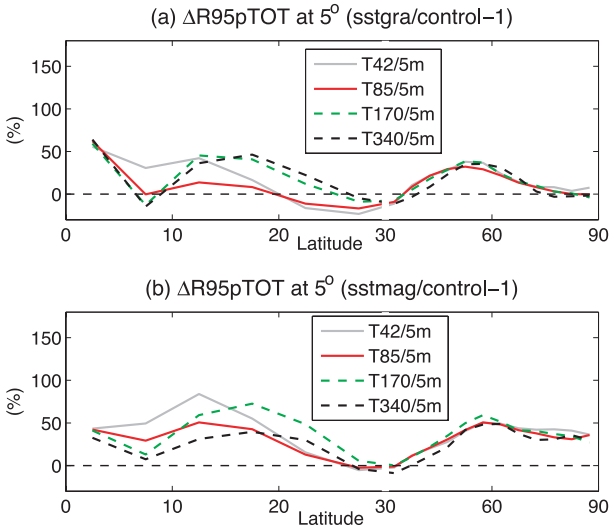

Fig. 5. The changes of extreme precipitation relative to control simulation for experiments under (a) 'sstgra' and (b) 'sstmag' scenarios. In contrast to the standard climate simulations with changing time steps, the model time steps are kept the same at 5 min for all the four horizontal resolutions. The precipitation has been averaged to coarser 5° grids before the statistics are calculated.

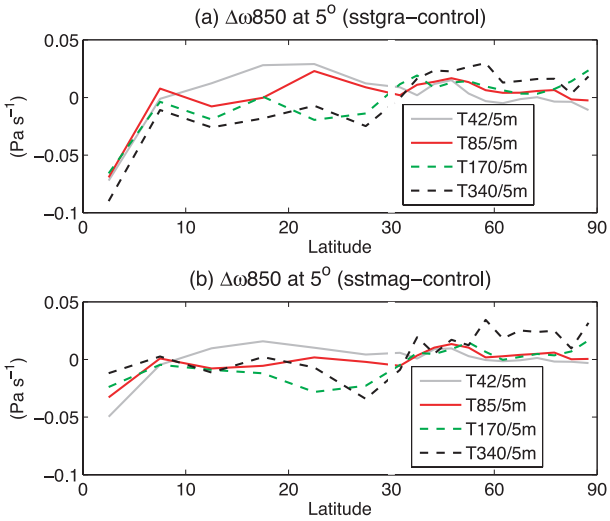

Fig. 6. The changes of 850 hPa ω (Pa s^{-1}) relative to control SST scenario, averaged to coarser 5° grids, at the same 5-min time step for all the four horizontal resolutions.

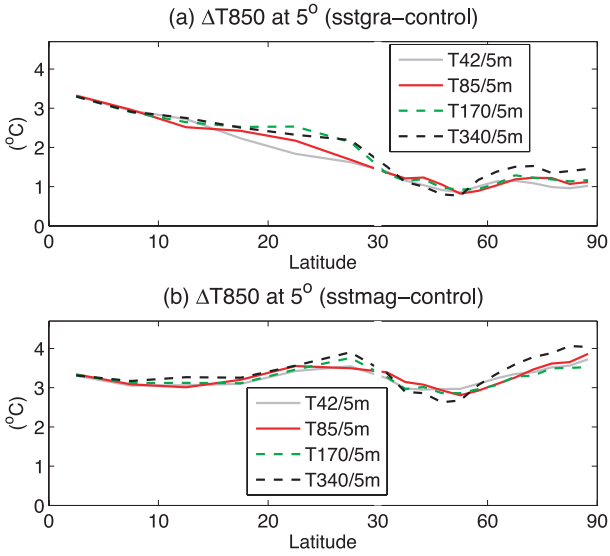

Fig. 7. The changes of 850 hPa temperature (°C) relative to control SST scenario, averaged to coarser 5° grids, at the same 5-min time step for all the four horizontal resolutions.

~70% increase for 'sstgra' and a ~50% increase for 'sstmag' scenarios (Fig. 5), although the extreme precipitation itself does not (Li et al., 2011). This suggests that the responses of extreme precipitation to horizontal resolution may have the same signs in the control and global warming experiments, and hence may have partially cancelled near the equator when subtracting the control from global warming experiments. This explanation is consistent with the fact that the tropical projections appear to be nearly independent of horizontal resolution.

3.5. *Changes of associated physical parameters*

Many studies have reported that extreme precipitation is associated updraft velocity and surface temperature (Allen and Ingram, 2002; O'Gorman and Schneider, 2009; Pall et al., 2007). These two parameters respectively are used to represent the 'dynamic' and 'thermodynamic' components of the drivers for extreme precipitation (Emori and Brown, 2005). We therefore plot the changes in the 850 hPa vertical velocity ω and in the 850 hPa temperature, during the days the extreme precipitation occur, relative to those in the control experiments at corresponding resolutions in Figs 6 and 7. The simulations are based upon a fixed time step of 5 min. we show the results at coarser 5 ° grids.

Stronger updrafts (negative ω) are associated with the increase of extreme precipitation under increased SST gradient scenario 'sstgra' at the equator (Fig. 6a). The changes in updraft velocity are consistent across different resolutions, although the sensitivity to resolution is more pronounced in the control simulations (not shown here; Li et al., 2011). The changes in updraft speed in experiment 'sstmag' are relatively small at the equator (Fig. 6b) and are consistent with the changes in extreme precipitation under this warming scenario (Fig. 5b), in which the changes of updraft velocities (negative ω) are correlated with the increase of extreme precipitation. The resolution dependence of the updraft is also small in this experiment.

In contrast to the updrafts, the changes in lower tropospheric temperature in these two global warming experiments show minimal sensitivity to resolution in the tropics. In the subtropical regions (20–30°), there is slight stronger warming for T170

and T340 compared with low-resolution runs for both warming scenarios, consistent with the extreme precipitation in Fig. 5. This implies that temperature changes during the extreme events may play a role in the extreme precipitation in this region (Emori and Brown, 2005). Although some resolution signals can be seen for lower tropospheric temperature in polar regions, the projections of extreme precipitation show little dependence on resolution primarily due to the very low mean and extreme precipitation rates (Fig. 5).

4. Conclusions

To aid in understanding the inconsistencies of the extreme precipitation projections across the climate models, a series of idealized AGCM runs using the 'aquaplanet' boundary conditions have been performed based on the Eulerian spectral transform Community Atmosphere Model CAM3 (Collins et al., 2004). Two simple global warming scenarios are defined with the simplest modifications of prescribed SST based on the SST profiles proposed by Neale and Hoskins (2000) in the Aqua-Planet Experiment Project protocol. The experiment 'sstgra' increases low-to-high latitude SST gradient through a 3 °C increase in the maximum SST at equator (eq. 2), and experiment 'sstmag' uniformly increases global SST magnitude by 3 °C (eq. 3). Although the two scenarios are not designed to represent the polar amplification projected for the actual climate, it is possible to derive useful information on the response of extremes to polar amplification through the comparison between 'sstgra' (larger latitudinal SST gradient) and 'sstmag' (smaller latitudinal gradient). Although the polar amplification would almost certainly enhance both the mean and extreme precipitation for polar regions, the smaller latitudinal gradient induced by polar warming may also mitigate the equatorial precipitation increase and the subtropical drying (inferred from the difference between 'sstgra' and 'sstmag', e.g. Fig. 5).

For a given resolution, the results show that, under the standard GCM simulation mode, the perturbed SSTs generally have stronger impacts on precipitation extremes compared with mean precipitation. Both warming scenarios show significant increases in extreme precipitation in the tropics and in the mid- to high latitudes. These findings are similar to those from the ensemble of six coupled ocean–atmosphere climate models established for IPCC AR4 report (Emori and Brown, 2005). The 'sstgra' warming scenario results in much stronger (up to 150%) increases in extreme precipitation at the equator than the increases observed in 'sstmag' experiment. In mid-latitude regions, the increases are comparable for the two experiments. The 'sstmag' experiment with higher SSTs everywhere produces much higher increases in extreme precipitation for polar regions where the SSTs are not increased under the 'sstgra' scenario. Experiment 'sstgra' also shows two regions with decreasing extreme precipitation near the equator and near the subtropical down-welling region that are not seen in the 'sstmag' experiment.

The projections of extreme precipitation to 'sstgra' warming scenario are affected by horizontal resolution in the low and middle latitudes, but not in high latitude regions. For 'sstmag', T85 tends to project higher extreme precipitation compared with other resolution runs under this warming scenario. The impact of horizontal resolution on the projections of extreme precipitation is small for the other three horizontal resolutions.

Further simulations have been performed for all the resolutions using the same time step to test the convergence of the large scales of the extreme precipitation projections under the 'sstgra' and 'sstmag' scenarios. The projections do not converge in the subtropics, although the signals are relatively noisy due to the very low precipitation rate in this region. Near the equator, the relative changes in the precipitation extremes in response to higher temperatures appear to converge although the unperturbed simulations of extreme precipitation do not (Li et al., 2011), the projections of extreme precipitation under global warming conditions appear to be independent of horizontal resolution when considering the same scale, that is averaged to the 5° grid.

Emori and Brown (2005) have pointed out that the change of vertical motion partly explains the tropical Pacific increase, although the change of precipitation and extremes in the mid-high latitudes are primarily due to 'thermodynamic' changes for given vertical motion. We show that stronger updraft is associated with the stronger increase of extreme precipitation at the equator in 'sstgra' experiment, compared with relatively smaller changes of both variables in experiment 'sstmag'. The changes of lower tropospheric temperature in these two global warming experiments show little resolution dependency at low-latitude regions. The small difference of lower tropospheric temperature across different resolutions at mid-latitudes could account for some of the divergence for the extreme precipitation projections in Fig. 5.

5. Acknowledgments

This work was supported by the Director, Office of Science, Office of Biological and Environmental Research, Climate Change Research Division, of the U.S. Department of Energy under Contract No. DE-AC02-05CH11231. Williamson and Olson were partially supported by the Office of Science (BER), U.S. Department of Energy, Cooperative Agreement No. DE-FC02-97ER62402. The National Center for Atmospheric Research is sponsored by the National Science Foundation.

References

Alexander, L. V., Zhang, X., Peterson, T. C., Caesar, J., Gleason, B. and co-authors. 2006. Global observed changes in daily climate extremes of temperature and precipitation. *J. Geophys. Res.* **111**, D05109, doi:10.1029/2005JD006290.

Allen, M. R. and Ingram, W. J. 2002. Constraints on future changes in climate and the hydrologic cycle. *Nature* **419**, 224–232.

Boyle, J. and Klein, S. A. 2010. Impact of horizontal resolution on climate model forecasts of tropical precipitation and diabatic heating for the TWP-ICE period. *J. Geophys. Res.* **115**, D23113, doi:10.1029/2010JD014262.

Chen, C. T. and Knutson, T. 2008. On the verification and comparison of extreme rainfall indices from climate models. *J. Clim.* **21**, 1605–1621.

Collins, W. D., Rasch, P. J., Boville, B. A., Hack, J. J., McCaa, J. R. and co-authors. 2004. Description of the NCAR Community Atmosphere Model (CAM3). Technical Note NCAR-TN−464+STR, National Center for Atmosphere Research, Boulder, CO.

Courant, R., Friedrichs, K. and Lewy, H. 1928. Über die partiellen Differenzengleichungen der mathematischen. *Physik* **100**(1), 32–74.

Courant, R., Friedrichs, K. and Lewy, H. 1967. On the partial difference equations of mathematical physics. *IBM J.* **11**, 215–234.

Cubasch, U., Meehl, G. A., Boer, G. J., Stouffer, R. J., Dix, M. and co-authors. 2001. Projections of future climate change. In: *Climate Change 2001: The Scientific Basis, Contribution of Working Group I to the Third Assessment Report of the Intergovernmental Panel on Climate Change* (eds. Houghton, J.T. et al.), Cambridge University Press, New York, 525–582.

Emori, S. and Brown, S. J. 2005. Dynamic and thermodynamic changes in mean and extreme precipitation under changed climate. *Geophys. Res. Lett.* **32**, L17706, doi:10.1029/2005GL023272.

Frich, P., Alexander, L. V., Della-Marta, P., Gleason, B., Haylock, M. and co-authors. 2002. Observed coherent changes in climatic extremes during the second half of the twentieth century. *Clim. Res.* **19**, 193–212.

Goswami, B. N., Venugopal, V., Sengupta, D., Madhusoodanan, M. S. and Xavier P. K. 2006. Increasing trend of extreme rain events over India in a warming environment. *Science* **314**, 1442–1445.

Held, I. M. and Soden B. J. 2006. Robust responses of the hydrological cycle to global warming. *J. Clim.* **19**, 5686–5699.

Lau, K. M. and Wu H. T. 2007. Detecting trends in tropical rainfall characteristics, 1979–2003. *Int. J. Climatol.* **27**, 979–988.

Li F., Collins W. D., Wehner M. F., Williamson D. L., Olson J. G. and Algieri C. 2011. Impact of horizontal resolution on simulation of precipitation extremes in an aqua-planet version of Community Atmospheric Model (CAM3). *Tellus A*, in press, DOI:10.1111/j.1600-0870.2011.00544.x.

Kharin, V. V., Zwiers F. W., Zhang, X. and Hegerl G. C. 2007. Changes in temperature and precipitation extremes in the IPCC ensemble of global coupled model simulations. *J. Clim.* **20**, 1419–1444.

Min, S.-K., Zhang, X., Zwiers, F. W. and Hegerl G. C. 2010. Human contribution to more intense precipitation extremes. *Nature* **470**, 378–381.

Neale R. B. and Hoskins B. J. 2000. A standard test for AGCMs including their physical parametrizations. I: The proposal. *Atmos. Sci. Lett.* **1**(2), 101–107, doi:10.1006/asle.2000.0022

O'Gorman, P. A. and Schneider, T. 2009. Scaling of precipitation extremes over a wide range of climates simulated with an idealized GCM. *J. Clim.* **22**, 5676–5685.

Pall, P., Allen, M. R. and Stone, D. A. 2007. Testing the Clausius–Clapeyron constraint on changes in extreme precipitation under CO2 warming. *Clim. Dyn.* **28**, 351–363, doi:10.1007/s00382-006-0180-2.

Randall, D. A., Wood, R. A., Bony, S., Colman, R., Fichefet, T. and co-authors. 2007. Climate models and their evaluation. In: *Climate Change 2007: The Physical Science Basis. Contribution of Working Group I to the Fourth Assessment Report of the Intergovernmental Panel on Climate Change* (eds. S. Solomon, D. Qin, M. Manning, Z. Chen, M. Marquis and co-editors), Cambridge University Press, Cambridge, UK and New York, NY, USA.

Schneider, T. and O'Gorman, P. A. 2007. Precipitation and its extremes in changed climates. In: *Extreme events: Proceedings of the 'Aha Huliko': a Hawaiian Winter Workshop*, University of Hawaii at Manoa, Honolulu, HI, 61–66.

Sun, Y., Solomon, S., Dai, A. and Portmann, R. W. 2006. How often will it rain? *J. Clim.* **20**, 4801–4818.

Trenberth, K. E. 1999, Atmospheric moisture recycling: role of advection and local evaporation. *J. Clim.* **12**, 1368–1381.

Trenberth, K. E., Dai, A., Rasmussen, R. M. and Parsons, D. B. 2003. The changing character of precipitation. *Bull. Amer. Meteor. Soc.* **84**, 1205–1217.

Williamson, D. L. 2008a. Equivalent finite volume and spectral transform horizontal resolutions established for aqua-planet simulations. *Tellus* **60A**, doi:10.1111/j.1600-0870.2008.00340.x.

Williamson, D. L. 2008b. Convergence of aqua-planet simulations with increasing resolution in the Community Atmospheric Model, Version 3. *Tellus* **60A**, 848–862.

Williamson, D. L. and Olson, J. R. 2003. Dependence of aqua-planet simulations on time step. *Quart. J. Roy. Meteor. Soc.* **129**, 2049–2064.

Wehner M. F., Bala, G., Duffy, P., Mirin, A. A. and Romano R. 2010. Towards direct simulation of future tropical cyclone statistics in a high-resolution global atmospheric model. *Adv. Meteorol.* **2010**, Article ID 915303, 13 pages, 2010, doi:10.1155/2010/915303.

Wilcox, E. M. and Donner, L. J. 2007. The frequency of extreme rain events in satellite rain-rate estimates and an atmospheric general circulation model. *J. Clim.* **20**, 53–69.